Neuroradiology (2002) 44: 371–381
DOI 10.1007/s00234-001-0760-0

W. Möller-Hartmann
S. Herminghaus
T. Krings
G. Marquardt
H. Lanfermann
U. Pilatus
F. E. Zanella

Clinical application of proton magnetic resonance spectroscopy in the diagnosis of intracranial mass lesions

Received: 10 August 2001
Accepted: 12 November 2001
Published online: 21 February 2002

W. Möller-Hartmann (✉) · T. Krings
Department of Neuroradiology,
University Hospital of Aachen
University of Technology,
Pauwelsstrasse 30, 52074
Aachen, Germany
E-mail: moeha@rad.rwth-aachen.de
Tel.: +49-241-8088345
Fax: +49-241-8888440

S. Herminghaus · H. Lanfermann
U. Pilatus · F.E. Zanella
Department of Neuroradiology,
University Hospital of Johann
Wolfgang von Goethe-University,
Schleusenweg 2–16,
60528 Frankfurt Main,
Germany

G. Marquardt
Clinic of Neurosurgery,
University Hospital of Johann
Wolfgang von Goethe-University,
Schleusenweg 2–16, 60528 Frankfurt
Main, Germany

Abstract Diagnosis of primary and secondary brain tumours and other focal intracranial mass lesions based on imaging procedures alone is still a challenging problem. Proton magnetic resonance spectroscopy (^{1}H-MRS) gives completely different information related to cell membrane proliferation, neuronal damage, energy metabolism and necrotic transformation of brain or tumour tissues. Our purpose was to evaluate the clinical utility of ^{1}H-MRS added to MRI for the differentiation of intracranial neoplastic and non-neoplastic mass lesions. 176 mostly histologically verified lesions were studied with a constant clinically available single volume ^{1}H-MRS protocol following routine MRI. 12 spectra (6.8%) were not of satisfactory diagnostic quality; 164 spectroscopic data sets were therefore available for definitive evaluation. Our study shows that spectroscopy added to MRI helps in tissue characterization of intracranial mass lesions, thereby leading to an improved diagnosis of focal brain disease. Non-neoplastic lesions such as cerebral infarctions and brain abscesses are marked by decreases in choline (Cho), creatine (Cr) and *N*-acetyl-aspartate (NAA), while tumours generally have elevated Cho and decreased levels of Cr and NAA. Gliomas exhibit significantly increased Cho and lipid formation with higher WHO tumour grading. Metastases have elevated Cho similar to anaplastic astrocytomas, but can be differentiated from high-grade gliomas by their higher lipid levels. Extra-axial tumours, i.e. meningiomas and neurinomas, are characterized by a nearly complete absence of the neuronal marker NAA. The additive information of ^{1}H-MRS led to a 15.4%-higher number of correct diagnoses, to 6.2% fewer incorrect and 16% fewer equivocal diagnoses than with structural MRI data alone.

Keywords Brain neoplasm · Glioma · Magnetic resonance spectroscopy · Cerebral infarction · Brain abscess

Introduction

The differential diagnosis of focal brain lesions depends on the ability of the experienced neuroradiologist to interpret a variety of rather indirect imaging criteria and clinical data. These include location, oedema, mass effect, calcification, cyst formation, vascularization, contrast enhancement, age and clinical presentation. The differentiation of ischaemic mass lesions, intra- and extra-axial brain tumours, and discrimination between high and low grade, however, often remains ambiguous if the diagnosis is exclusively based on these criteria [1, 2, 3, 4, 5].

In contrast to MRI, CT, and angiography, i.e. methods that provide structural data, proton magnetic resonance spectroscopy (^{1}H-MRS) gives completely

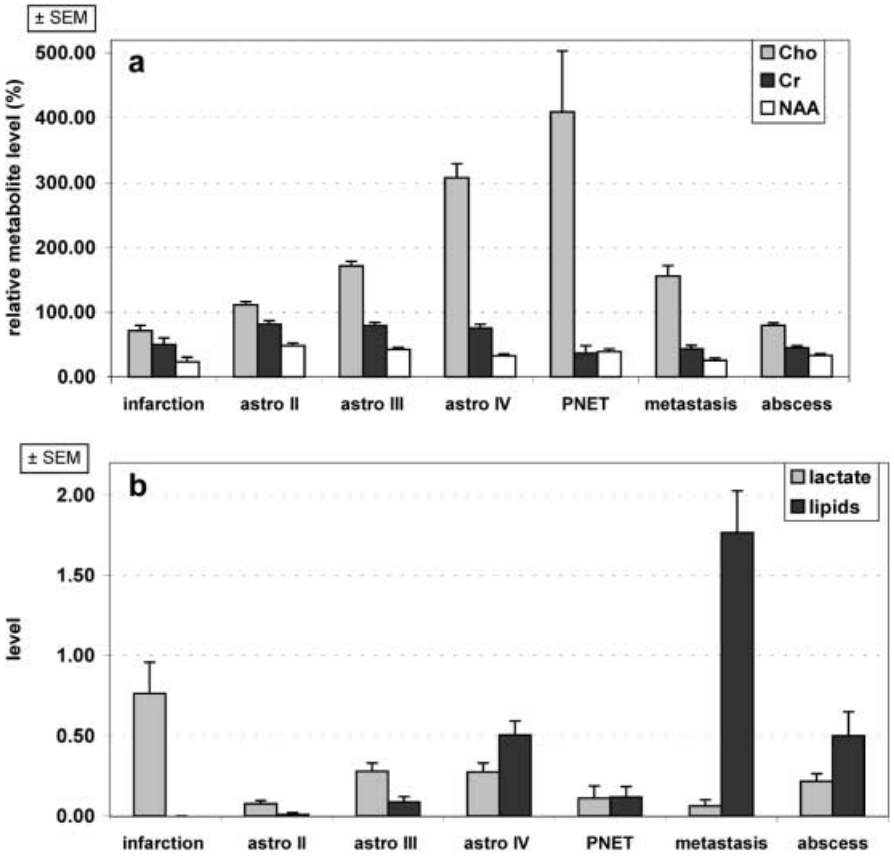

Fig. 1. **a** Relative metabolite levels of Cho, Cr and NAA expressed as percentage of mass lesion/contralateral brain metabolite proportion. All brain lesions have diminished NAA and Cr. Cho is generally decreased in non-neoplastic brain lesions (infarction, abscess) and elevated in brain tumours. Note the statistically significant increase of Cho in gliomas according to tumour grading. In comparison with gliomas, metastases show decreased NAA and Cr, while Cho levels of metastases are in the range of anaplastic astrocytomas. **b** Signal intensities of lactate (Lac) and lipids (Lip) expressed as ratio to Cr of contralateral reference spectrum (i.e. Lac and Lip level). Infarctions are characterized by prominent lactate resonances. Glioblastomas exhibit higher lipid levels than anaplastic astrocytomas and low-grade gliomas. The highest lipid levels are observed in metastases, with statistically significant differences from anaplastic astrocytomas, glioblastomas and all other intracranial mass lesions. *Astro II* astrocytoma WHO II, *astro III* anaplastic astrocytoma WHO III, *astro IV* astrocytoma (glioblastoma) WHO IV, *PNET* primitive neuroectodermal tumour (medulloblastoma), *Cho* choline, *Cr* creatine, *NAA* *N*-acetyl-aspartate, *SEM* standard error of mean

different information related to neuronal integrity [6], cell proliferation or degradation [7, 8, 9], energy metabolism [6], and necrotic transformation of brain or tumour tissues [10]. Hence, in conjunction with structural imaging modalities, ^{1}H-MRS is playing an increasingly important role in a number of common neurological disorders such as stroke, epilepsy, multiple sclerosis, HIV, dementia, head injury and near drowning [11]. Although numerous ^{1}H-MRS studies have been conducted in order to describe metabolic patterns of focal brain lesions [12, 13, 14, 15, 16], only a few investigations focussed on the complementary differential diagnostic value of ^{1}H-MRS added to MRI or other imaging methods [17, 18]. In particular, the clinical utility of ^{1}H-MRS for solving key diagnostic problems, e.g. differentiation between neoplastic and non-neoplastic lesions, low- and high-grade tumours, infarction and low-grade gliomas, or separating metastases from primary brain tumours and abscesses, has not yet been defined in a large series of patients. In the present study, metabolic patterns of focal brain lesions were reviewed with regard to their potential impact for overcoming the aforementioned problems.

Methods and materials

This is a consecutive series of 176 patients who presented to the department of neuroradiology with focal intracranial mass lesions. All patients were investigated under a constant single-volume ^{1}H-MRS protocol following structural MRI and/or CT imaging. All imaging and spectroscopic studies were carried out with a 1.5-T whole-body magnetic resonance scanner (Magnetom Vision, Siemens) using a circularly polarized head coil. While all structural MRI data were acquired in satisfactory imaging quality, the spectra of 12 patients (6.8%) could be obtained only in poor quality, without any diagnostic significance, mostly due to movement artefacts and/or non-compliance on the part of the patients;

therefore, 164 spectroscopic data sets were available for further assessment (Fig. 1; Table 2).

Within 10 days of spectroscopic examination, histological diagnosis was obtained by stereotactic biopsy or craniotomy and open biopsy, except in 9 (of 25) cases of brain abscesses or focal inflammatory brain disease and 9 (of 9) cases of cerebral infarction. The diagnoses in these patients were based on magnetic resonance and CT features, clinical course, cerebrospinal-fluid findings and blood laboratory tests. Patients with cerebral infarction were examined during the acute and subacute phases with onset of clinical symptoms of less than 72 h.

Definitive diagnoses (of the patients with successfully completed MRI and MRS) included 23 low-grade astrocytomas (WHO II), 28 anaplastic astrocytomas (WHO III), 39 glioblastomas (WHO IV), 4 PNETs or medulloblastomas, 18 metastases, 9 meningiomas, 9 neurinomas, 25 cerebral abscesses and 9 brain infarctions.

The MRI and spectroscopic findings were reviewed independently by various experienced readers, who were blinded for the definitive diagnosis: Two readers (W.M.H., S.H.) made their diagnosis based on data from MRI and MRS, while two other investigators (H.L., F.E.Z.) made their diagnosis by interpreting the magnetic resonance images alone (without the added information given by MRS). A diagnosis was voted as "correct" if, not only the kind of intracranial mass lesion (i.e. metastasis, abscess, glioma, meningioma, neurinoma, infarction etc.), but also the tumour grading according to the WHO classification, was diagnosed correctly. If the neuroradiologists could not decide between several differential diagnoses, this was considered as "no evident diagnosis" (Table 2).

Proton magnetic resonance spectroscopy

To guide single-voxel spectroscopic examinations, scout magnetic resonance images using either contrast-enhanced T1-weighted or T2-weighted two-dimensional gradient-echo sequences were obtained in exact axial, coronal and sagittal planes. Afterwards, a volume of interest (VOI) of 4–12 ml (mean: 8 ml) was placed in the solid part of the mass lesion excluding necrotic or cystic tumour parts or adjacent oedematous brain. For this study, we accepted any patient with an estimated tumour fraction in the magnetic resonance spectroscopy voxel greater than 70%. Whenever feasible, identical VOIs were acquired from a homologous region of the contralateral hemisphere. To avoid partial volume artefacts with internal and external liquor spaces, which would reduce the effective voxel size of brain metabolites, we placed the contralateral voxel into the white matter (reference spectrum). In cases of lesions located in the midline or in the cerebellar vermis, the reference spectrum was taken from the left parieto-occipital white-matter region. Water-suppressed single-voxel spectra were acquired using a double spin-echo localization technique (PRESS, point-resolved excitation spin-echo sequence) with frequency-selective water suppression. The PRESS sequence was used with parameters of 1,500/135 (TR/TE) because of sufficient signal-to-noise ratio reported for the PRESS technique and in order to minimize phase-induced baseline distortion [19, 20]. Depending on the size of the selected VOI, either 128 or 256 acquisitions were performed, leading (at a TR of 1,500 ms) to a total pure acquisition time of 3 min 15 s up to 6 min 30 s per voxel. Prior to spectroscopic acquisition, global and localized shimming on the water proton as well as optimization of water suppression was performed, resulting in an overall spectroscopic examination time of 30–60 min for both voxels.

Postprocessing and analysis of spectroscopic data

Time domain data were multiplied with a Gaussian function (centre 0, half width 256 ms), 2D Fourier transformed, phase and baseline corrected and quantified by means of frequency domain curve fitting with the assumption of a Gaussian line shape using the NUMARIS-3 software package (Siemens). Obtained metabolite signals centred at 0.9, 1.3, 1.5, 2.0, 3.0 and 3.2 ppm were attributed to aliphatic lipids (Lip) (fatty acid-CH_2 and -CH_3), lactate (Lac), alanine (Ala), *N*-acetyl-aspartate (NAA), creatine/phosphocreatine (Cr) and choline (Cho) [21]. At a TE of 135 ms Lac can be differentiated from lipids, because Lac-bound protons are dephased and therefore exhibit an inverted j-coupled double peak at 1.3 ppm (with a narrow bandwidth that is comparable with the peaks of the other metabolites), whereas lipids exhibit broad peaks at 1.3 ppm without phase reversal [10, 15]. Tumour metabolite signal intensities were quantified (or normalized) in two different ways. First, the peak area signal intensity of each metabolite (NAA, Cr and Cho) in the lesion was expressed as percentage of the corresponding metabolites of the reference spectrum (these values will be further referred to as "relative signal intensity" or "metabolite level"). Assuming brain metabolites to have an appropriate internal concentration standard, this permits semi-quantitative estimation of the extent to which metabolite concentrations are altered in focal brain lesions [15]. Lip and Lac, which are not detectable in normal brain, were normalized using Cr of the contralateral reference spectrum as an internal standard (these values will be referred to as "Lip level" and "Lac level"). The second way in which we quantified our data was by expressing the peak area intensities of the metabolites NAA and Cho as ratios to intratumoral Cr (Cho/Cr or NAA/Cr ratio).

Statistics

After statistical evaluation for normal distribution (Kolmogorov-Smirnov test), we used Student's *t*-test for non-paired group comparison for analysis of data. The level of significance was determined at $P \leq 0.05$.

Results

Intra-axial neoplastic lesions

All gliomas showed increased Cho and reduced NAA compared with normal brain (1a; Table 1). According to tumour grading, the relative signal intensities of Cho and Cho/Cr ratio showed a statistically significant increase from low-grade astrocytoma to anaplastic astrocytoma to glioblastoma (Figs. 1a, 2, 3, 4; Table 1). The highest Cho levels were observed in PNETs (Figs. 1a, 5; Table 1). NAA was reduced in all gliomas; again, corresponding to tumour grade, there was a statistically significant decline in the signal intensity of NAA that correlated inversely with the tumour grade.

Cr was moderately decreased in all gliomas, without statistically significant differences between low- and high-grade gliomas (Fig. 1a; Table 1). Remarkable is the strong statistically significant decrease of Cr signal intensity in PNET tumours compared with low- and high-grade astrocytomas (Fig. 1a; Table 1). Due to the diminished Cr level, the NAA/Cr ratio of PNET tumours was statistically significantly higher than those of low- and high-grade gliomas (Table 1).

Low-grade gliomas had no or only low Lac and Lip. With increasing malignancy, tumours exhibited Lac and prominent Lip peaks, with statistically significant differences for Lip between low-grade astrocytomas, anaplastic astrocytomas and glioblastomas (Figs. 1b, 2, 3, 4). There were no noteworthy resonances of Lip or Lac in PNET tumours (Fig. 5).

Metastases

In metastases the signal intensities of Cho were increased to values comparable with anaplastic astrocytomas (Figs. 1a, 6; Table 1). Signal intensities of NAA and Cr were statistically significantly lower than in low- and high-grade astrocytomas (Fig. 1a; Table 1). Because of reduced Cr signal intensity, Cho/Cr ratios of metastases were statistically significantly higher than those of anaplastic astrocytomas (Table 1). Beside this findings, metastases showed strongly elevated Lip, with statistically significant differences from glioblastomas, anaplastic astrocytomas, abscesses and all other intracranial mass lesions (Figs. 1b, 6).

Extra-axial neoplastic lesions

Spectra of meningiomas and neurinomas were characterized by prominent Cho resonances (Fig. 7). The relative signal intensities of Cr and NAA were strongly decreased, and NAA especially was seldom identified (Fig. 7; Table 1). Six of nine meningiomas showed a dephased double peak at 1.5 ppm, which is attributed to Ala [13]. Alanine was not visible in any neurinomas or other brain lesion. Compared with contralateral brain, neurinomas showed only slight increases of Cho, whereas meningiomas showed moderate increases of Cho signal intensities (Table 1). Because both tumour entities had strongly decreased Cr peaks (Table 1), meningiomas and neurinomas had notably elevated Cho/Cr ratios (Table 1). There

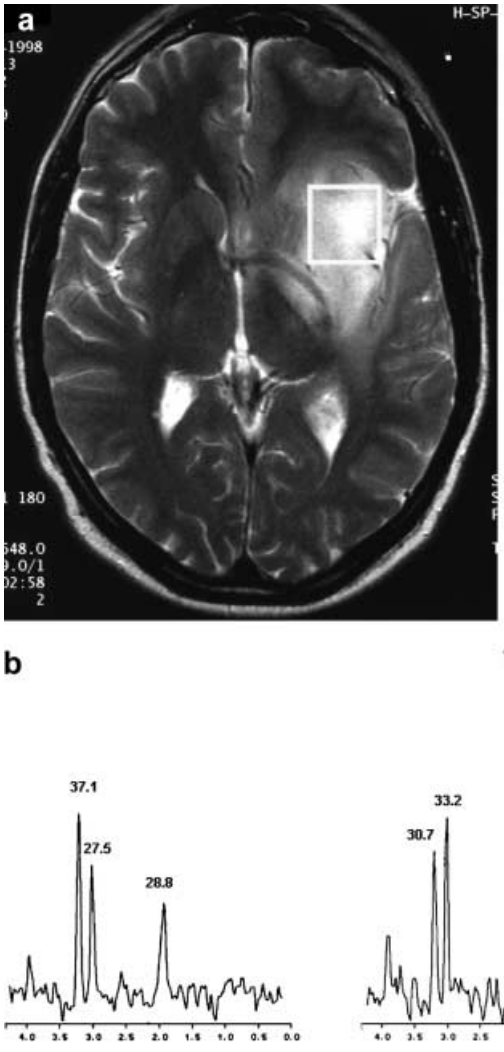

Fig. 2a, b. Astrocytoma WHO II. **a** Location. **b** *Left spectrum*: mass lesion. *Right spectrum*: contralateral brain. Values at top of NAA (2.0 ppm), Cr (3.0 ppm) and Cho (3.2 ppm) reflect signal peak integrals (arbitrary units). Metabolite levels relative to contralateral brain: NAA 38%; Cr 83%; Cho 120%. Levels of NAA and Cr are decreased while Cho is moderately elevated in low grade gliomas

Table 1. Metabolite/Cr ratios (Cho/Cr and NAA/Cr) and percental signal intensities of Cho, Cr and NAA relative to reference spectrum (i.e. healthy tissue on contralateral hemisphere). The table displays mean values ± standard error of mean

Lesion	Cho/Cr	NAA/Cr	Cho (%)	Cr (%)	NAA (%)
Infarction[a]	1.45 ± 0.22	0.93 ± 0.25	71.0 ± 8.3	49.9 ± 10.5	23.3 ± 6.9
Astrocytoma II	1.33 ± 0.08	1.14 ± 0.10	111.2 ± 5.0	80.9 ± 5.5	48.2 ± 4.4
Astrocytoma III	2.13 ± 0.12	1.02 ± 0.06	170.9 ± 7.5	78.7 ± 5.2	42.5 ± 2.7
Astrocytoma IV	3.93 ± 0.64	0.92 ± 0.11	307.7 ± 21.4	75.2 ± 6.1	32.8 ± 2.2
PNET	18.4 ± 6.30	4.73 ± 2.59	409.3 ± 93.8	36.3 ± 11.8	39.0 ± 4.1
Metastasis	3.97 ± 0.74	1.09 ± 0.23	155.5 ± 16.2	43.2 ± 5.4	25.2 ± 4.2
Abscess	1.52 ± 0.10	1.26 ± 0.10	79.5 ± 3.9	44.9 ± 3.3	33.1 ± 3.1
Meningioma[b]	4.81 ± 1.04	1.20 ± 0.37	137.4 ± 13.2	26.9 ± 7.2	12.7 ± 3.5
Neurinoma	3.08 ± 0.78	0.55 ± 0.15	112.0 ± 6.4	38.6 ± 9.8	11.8 ± 3.9

[a]Five of nine infarct spectra exhibited an additional acetate peak
[b]Six of nine meningiomas exhibited an additional alanine peak

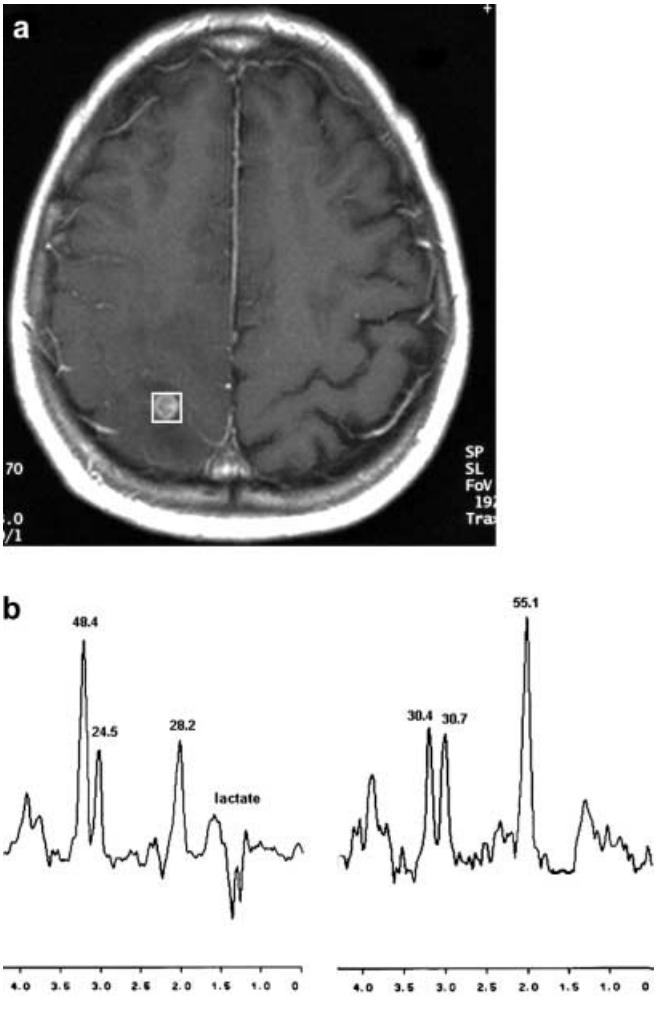

Fig. 3a, b. Astrocytoma WHO III. **a** Location. **b** *Left spectrum*: mass lesion. *Right spectrum*: contralateral brain. Values at top of NAA (2.0 ppm), Cr (3.0 ppm) and Cho (3.2 ppm) reflect signal peak integrals (arbitrary units). Metabolite levels relative to contralateral brain: NAA 51%; Cr 79%; Cho 159%. Note the dephased lactate peak (caused by anaerobic glycolysis) at 1.3 ppm and increasing Cho level according to WHO tumour grading in this case of anaplastic astrocytoma

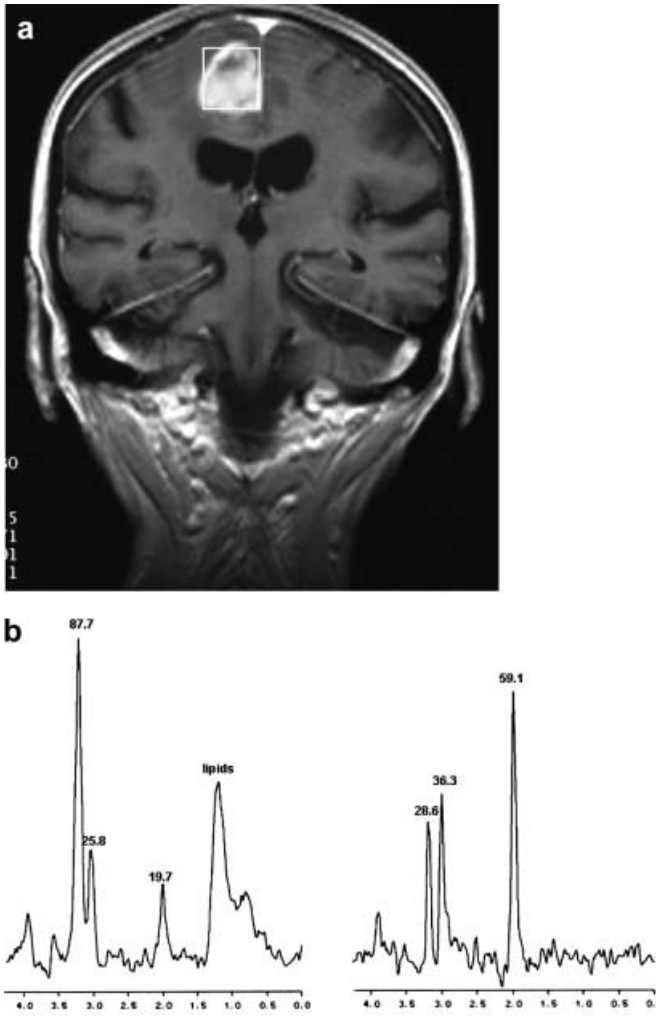

Fig. 4a, b. Astrocytoma WHO IV (GBM). **a** Location. **b** *Left spectrum*: mass lesion. *Right spectrum*: contralateral brain. Values at top of NAA (2.0 ppm), Cr (3.0 ppm) and Cho (3.2 ppm) reflect signal peak integrals (arbitrary units). Metabolite levels relative to contralateral brain: NAA 33%; Cr 71%; Cho 306%. There is a further increase of Cho proportional to tumour grading in grade IV gliomas. Broad lipid resonances at 1.3 and 0.9 ppm are due to micro- and macronecrosis, one of the microscopic hallmarks of GBM

were only unremarkable Lac and Lip resonances in meningiomas and neurinomas.

Non-neoplastic lesions

Brain abscesses (Figs. 1a, 8; Table 1) showed decreased levels of Cho, Cr and NAA. The Cho levels were statistically significantly lower than those of the contrast-enhancing neoplasms, i.e. anaplastic astrocytomas, glioblastomas, PNETs and metastases. Abscesses exhibited moderate Lip resonances at 1.3 ppm (fatty acid-CH_2) and occasionally at 0.9 ppm, which are assigned to cytosolic amino-acid residues [22] or to fatty acid-CH_3 resonances [23], and to a lesser extent, Lac. Especially, abscesses of tuberculous origin expressed high Lip.

Cerebral infarction showed strong and homogeneous decrease of all metabolites, with statistically significant reductions of Cho, NAA and Cr compared with low- and high-grade gliomas (Figs. 1a, 9; Table 1). Because all metabolites including Cr were reduced in ischaemia, Cho/Cr and NAA/Cr ratios of brain infarction did not differ from the Cho/Cr and NAA/Cr ratios of low-grade gliomas (Table 1). According to the ischaemic origin of infarction all infarct spectra exhibited high Lac resonances, while Lip was not observed (Figs. 1b, 9).

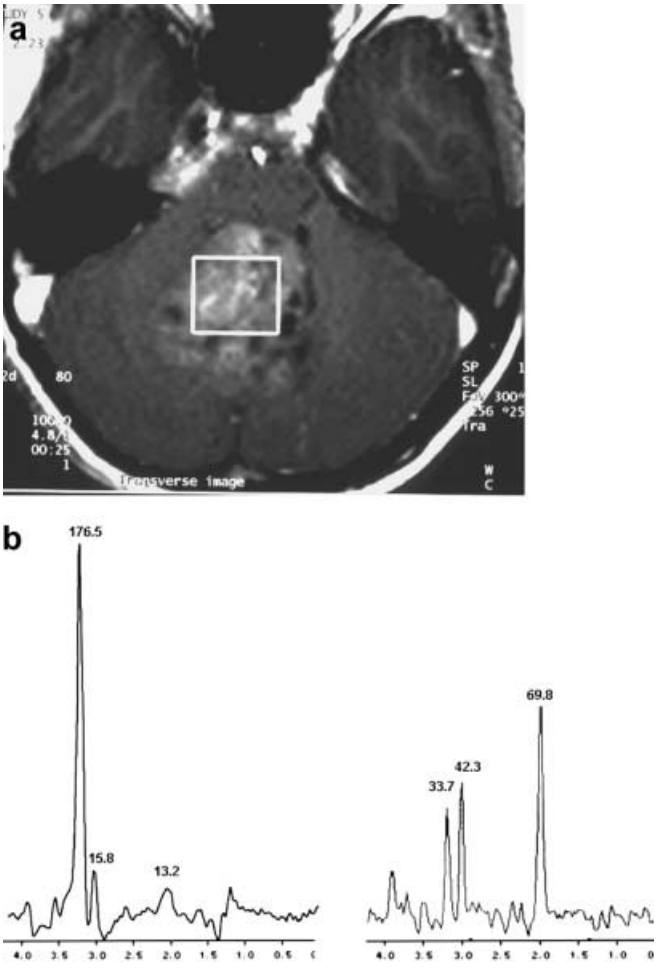

Fig. 5a, b. PNET (medulloblastoma). **a** Location. **b** *Left spectrum*: mass lesion. *Right spectrum*: normal healthy brain. Values at top of NAA (2.0 ppm), Cr (3.0 ppm) and Cho (3.2 ppm) reflect signal peak integrals (arbitrary units). Metabolite levels relative to contralateral brain: NAA 19%; Cr 37%; Cho 524%. In our series, PNETs showed the highest Cho levels of all brain tumours

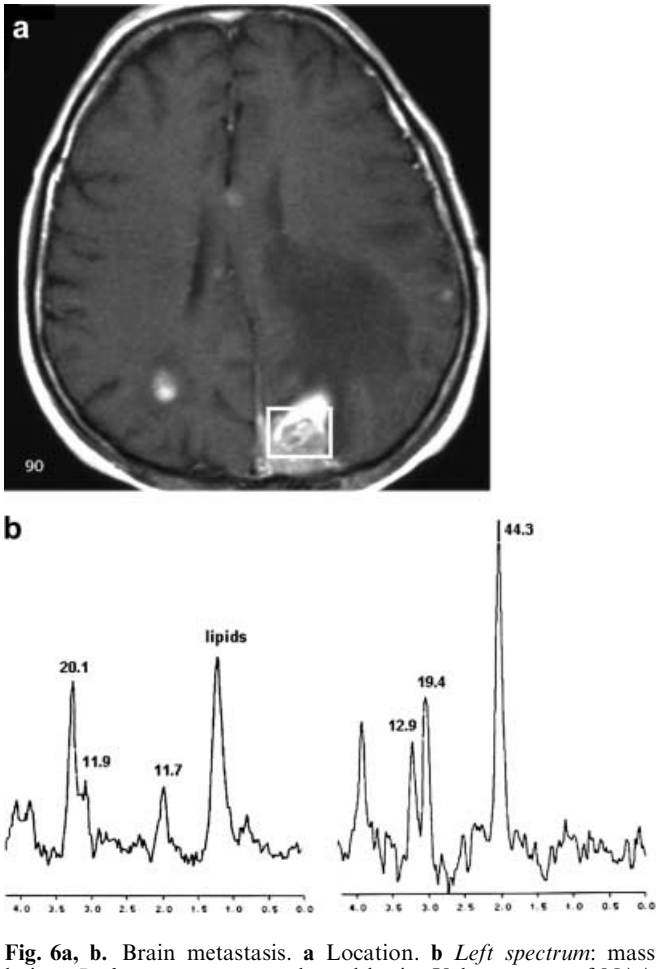

Fig. 6a, b. Brain metastasis. **a** Location. **b** *Left spectrum*: mass lesion. *Right spectrum*: contralateral brain. Values at top of NAA (2.0 ppm), Cr (3.0 ppm) and Cho (3.2 ppm) reflect signal peak integrals (arbitrary units). Metabolite levels relative to contralateral brain: NAA 26%; Cr 61%; Cho 156%. Note broad lipid resonances at 1.3 (fatty-acid methylene-group) and 0.9 ppm (fatty-acid methyl-group). Spectra of metastasis are characterized by elevated Cho and prominent lipid peaks. Lipid resonances in metastasis are due to mobile membrane-bound lipids and occur even in absence of necrosis

In five (of nine) cerebral infarctions, there was an additional peak at 1.8 ppm, which is attributed to acetate [22, 24].

Diagnostic value of ^{1}H-MRS added to MRI

With conventional MRI alone 97 (of 176) correct diagnoses (including the accurate WHO grade classification) were made (55.1%). ^{1}H-MRS in addition to MRI led to the correct diagnosis in 124 (of 176) cases (70.5%); the rate of correct diagnoses was therefore raised by 15.4% when the diagnostic information of MRS was added to that of MRI (Table 2).

The number of incorrect diagnoses could be lowered from 27 (15.3%) for MRI alone to 16 (9.1%) for ^{1}H-MRS in addition to MRI. The cases without evident diagnoses were diminished from 52 (29.6%) to 24 (13.6%). In no patient was a correct diagnosis established by MRI alone interpreted incorrectly by the combined use of ^{1}H-MRS and MRI. In 12 patients (6.8%) the MRS examinations were of no diagnostic value, while all MRI scans were of sufficient diagnostic quality.

Discussion

In spite of the fact that the function of NAA is not known exactly, it is generally recognized as a marker of functional neurons and their appendages (including dendrites) [12, 15, 25]. Whenever brain tissue is damaged or

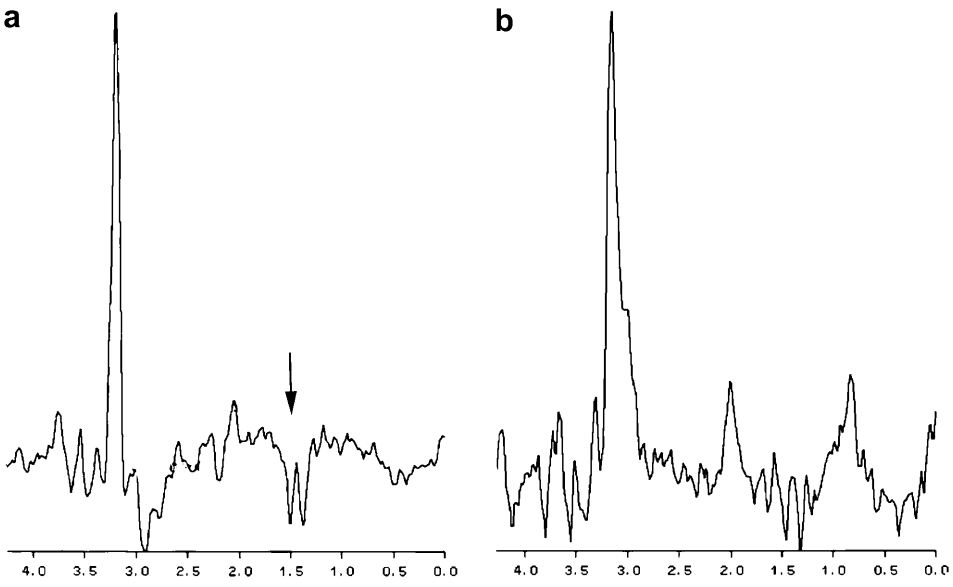

Fig. 7. **a** Meningioma; **b** neurinoma. Spectra are characterized by a Cho mono-peak (3.2 ppm) and no or only low resonances of NAA (2.0 ppm) and Cr (3.0 ppm). Note dephased alanine peak at 1.5 ppm in meningioma (*arrow*) and small lipid peak (fatty-acid methyl-group) at 0.9 ppm in neurinoma

replaced by any destructive, degenerative or infiltrative process, NAA is markedly reduced. Extra-axial lesions, which do not infiltrate brain or which do not contain neuroglial tissue, will not demonstrate any NAA resonances [8, 12, 13, 15, 18, 26]. Since Cr-bound phosphates are a substrate of the ATP/ADP cycle, Cr is considered to be an indicator of energy metabolism. Because Cr is quite constant in various metabolic conditions, it has often been used as an internal standard for semi-quantitative evaluation of metabolic changes of other brain metabolites [15, 27, 28]. Cho resonances originate mainly from intermediates of phospholipid metabolism such as phosphocholine and glycerophosphocholine, which both play an important role in the structure and function of cell membranes [23, 29]. Consequently, increased Cho can be seen in processes with elevated cell-membrane turnover, such as in proliferating tumours and in developing brain [30]. Lipids and lactate are physiologically not detectable in healthy brain. In-vitro studies have shown that the amount of lipids detected by spectroscopy correlates well with the degree of micro- and macronecrosis [10] seen on histology. Brain lactate is produced in conditions of anaerobic glycolysis, i.e. during a mismatch between glycolysis and oxygen supply, and indicates hypoxic conditions as well as hypermetabolic glucose consumption [31, 32].

In accordance with several former studies [18, 33, 34, 35, 36, 37], we observed as a common feature of primary and metastatic brain tumour increased Cho and decreased NAA (Fig. 1a; Table 1). Non-neoplastic lesions such as cerebral infarction and brain abscess, on the other hand, showed markedly decreased Cho resonances. Therefore, Cho as a marker of proliferating tissue can differentiate between neoplastic lesions (elevated Cho) and non-neoplastic tissue (decreased Cho).

Histopathological tumour grades of gliomas can be determined reliably with relatively simple, clinically available techniques for acquisition and analysis of brain spectra. These findings are in general concordance with previous works [16, 18, 37]. According to the grade of malignancy in gliomas, there was a statistically significant increase in Cho, i.e. Cho was the best index for grading cerebral gliomas according to WHO criteria (Fig. 1a; Table 1); these findings correlate well with recently published data [16, 38, 39], which showed a positive correlation of Cho/Cr ratios with the histological grading of astrocytomas and the labelling index of KI-67, a histochemically detectable proliferation marker. Glioblastomas exhibited statistically significantly higher lipid levels than low-grade astrocytomas and anaplastic astrocytomas. Since necrosis is (besides mitotic activity of tumour cells and presence of vascular glomeruli) one of the microscopic hallmarks of glioblastomas [38], spectroscopic detection of lipids is, therefore, not surprising. The amount of lipids was the second-best discriminator between low- and high-grade gliomas, while changes of Cr and NAA signal intensities were less helpful in grading cerebral gliomas. Medulloblastomas (PNET-tumours) showed the highest Cho signal intensities in our series (with statistically significant differences from high-grade gliomas), decreased NAA and Cr and unremarkable resonances of lactate and lipids. These findings reflect well the clinical course of medulloblastomas as fast-growing tumours with a high proliferation rate.

Metastases are known to show variably increased Cho and low Cr and NAA [12, 14, 33]. Additionally, metastases apparently exhibit prominent lipid resonances [13, 35]. In our series, metastases showed unique spectroscopic findings, which differentiated them

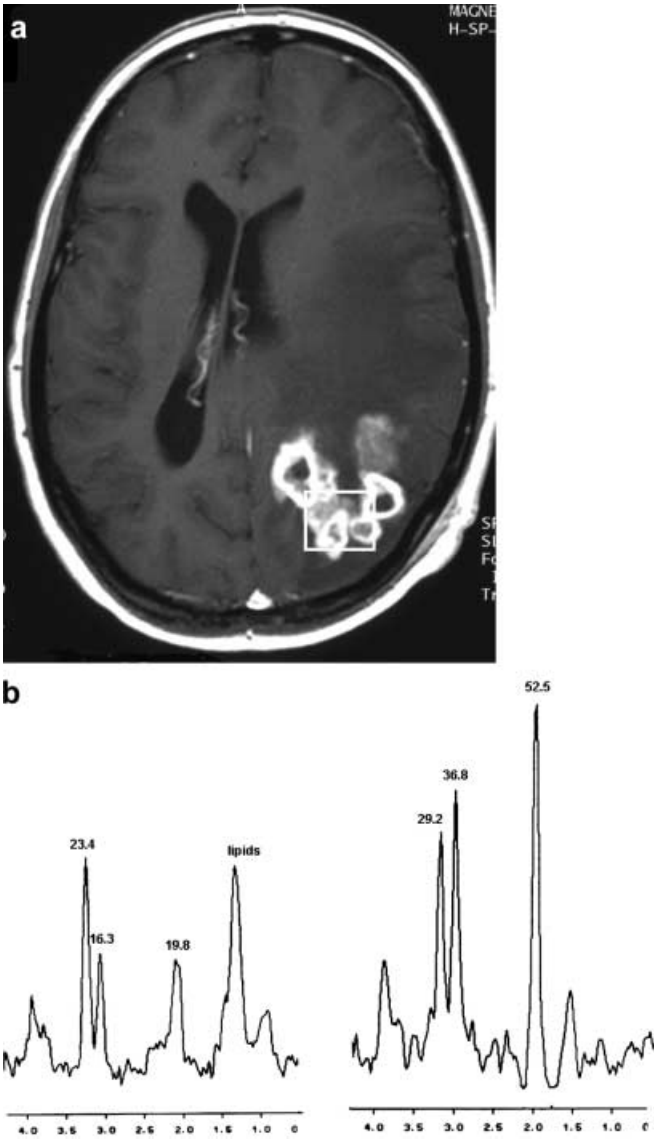

Fig. 8a, b. Brain abscess. **a** Location. **b** *Left spectrum*: mass lesion. *Right spectrum*: contralateral brain. Values at top of NAA (2.0 ppm), Cr (3.0 ppm) and Cho (3.2 ppm) reflect signal peak integrals (arbitrary units). Metabolite levels relative to contralateral brain: NAA 38%; Cr 44%; Cho 80%. Resonances at 1.3 ppm and 0.9 ppm are due to lipids. In contrast to metastases, high-grade gliomas and other neoplastic lesions, Cho levels are decreased in inflammatory brain disease

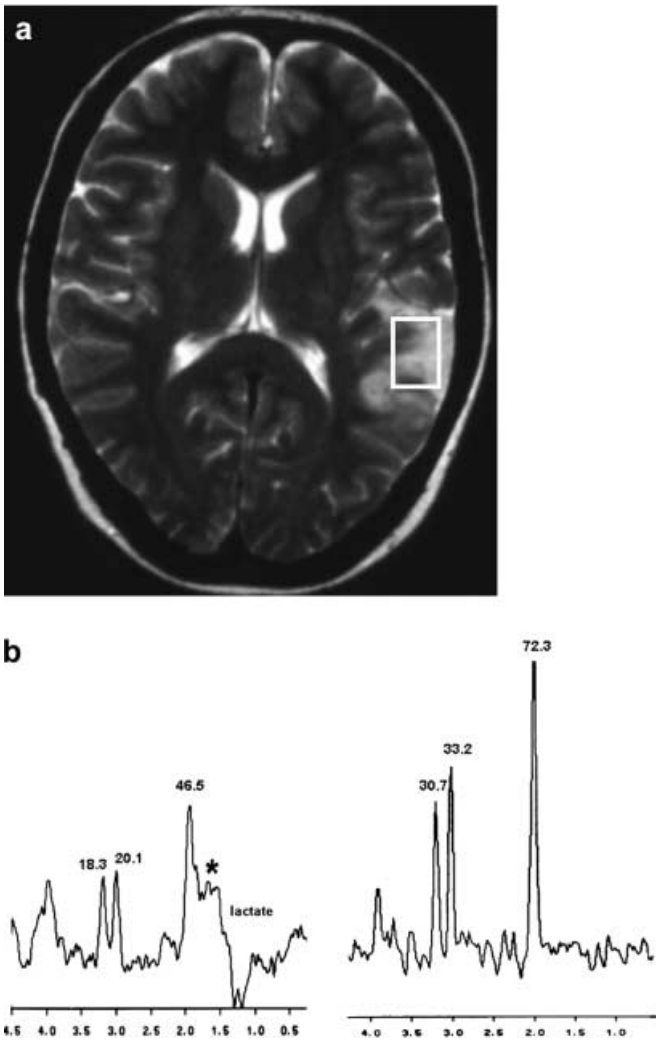

Fig. 9a, b. Cerebral infarction. **a** Location. **b** *Left spectrum*: lesion. *Right spectrum*: contralateral brain. Values at top of NAA (2.0 ppm), Cr (3.0 ppm) and Cho (3.2 ppm) reflect signal peak integrals (arbitrary units). Metabolite levels relative to contralateral brain: NAA 64%; Cr 61%; Cho 59%. All brain metabolites (including Cho) are decreased. Note prominent phase reversed lactate resonances at 1.3 ppm and the acetate peak at 1.8 ppm (*)

from other contrast-enhancing neoplastic and non-neoplastic masses (Figs. 1, 6; Table 1). In comparison with brain abscesses, metastases had elevated Cho peaks, whereas the contrast-enhancing parts of inflammatory brain disease showed decreased Cho. Metastases were characterized by Cho levels comparable with anaplastic astrocytomas, but in contrast to high-grade gliomas, metastases showed – even in the absence of necrosis – markedly higher lipid levels. NAA and Cr were significantly lower in metastases than in gliomas, which can be explained by the displacing growth of metastases rather than the more infiltrating growth of gliomas [13]. Mountford and co-workers [40, 41] give a possible explanation for elevated lipids in metastatic lesions: cancer cells of different origin, which have the potential to metastasize, contain mobile spectroscopically detectable lipids in their cell membranes, while cell cultures of tumours which do not lead to metastases do not exhibit these mobile membrane-bound lipids. Thus, the uniform appearance of brain metastases of different origin is well explained by the fact that metastasizing tumour

Table 2. The data display the additional information of ^{1}H-MRS (^{1}H-MRS + MRI) in comparison with structural imaging (MRI) alone. The proportion of correct diagnoses is 15.4% higher when the diagnosis is based on ^{1}H-MRS + MRI instead of MRI solely. The number of incorrect diagnoses is reduced by 6.2% and the number of cases without evident diagnosis by 14% when the complementary diagnostic information of ^{1}H-MRS is used

Procedure	Correct diagnosis	Incorrect diagnosis	No evident diagnosis	Examination without diagnostic value
	Number (%)	Number (%)	Number (%)	Number (%)
MRI	97 (55.1)	27 (15.3)	52 (29.6)	0 (0)
^{1}H-MRS + MRI	124 (70.5)	16 (9.1)	24 (13.6)	12 (6.8)

cells contain a higher amount of membrane-bound lipids than non-metastasizing cancer cells [42].

Meningiomas and neurinomas are extra-axial tumours. Therefore, it is not surprising that both extra-axial neoplasms showed absent or only low NAA in our series (Fig. 7; Table 1); the presence of NAA in extra-axial masses is attributed to contamination of the voxel with adjacent brain tissue and to partial volume artefacts and does not reflect the presence of NAA in meningiomas or neurinomas [12, 13, 29]. Cho/Cr ratios of meningioma and neurinomas were strongly elevated, due to the fact that the relative signal intensities of Cr in both tumours were clearly diminished (Fig. 7; Table 1). In these tumours Cho/Cr ratios should therefore not be used for purposes of tumour grading. Meningiomas exhibited higher Cho levels than neurinomas, but the most obvious discriminating factor for differentiating meningiomas from neurinomas was the presence or absence of Ala, which is represented by a dephased j-coupled double peak at 1.5 ppm (Fig. 7). According to the literature [13, 26, 29], we could find Ala in six of the nine meningiomas studied; we did not observe Ala in any case of the nine examined neurinomas in this series. Thus, the presence of Ala in meningiomas seems to be useful for differentiating them from neurinomas in diagnostically difficult cases. On the other hand, the presence of lactate and lipids, which is probably attributable to small areas of cystic tumour degeneration often evident on magnetic resonance scans in neurinomas, did not help to distinguish neurinomas from meningiomas.

Besides reduced NAA and Cr, abscesses demonstrated markedly decreased Cho levels with statistically significant differences from metastases and gliomas (Figs. 1a, 8; Table 1). As reported by other authors, we found strong lipid resonances, especially in abscesses of tuberculous origin or in cases of toxoplasmosis [43]. Our aim was to characterize brain lesions by spectroscopy of the solid part, avoiding partial volume artefacts from cystic or necrotic areas, and our data indicate that spectra of contrast-enhancing lesions with decreased Cho, NAA and Cr are typical for brain abscesses. We did not study the spectroscopic findings in cystic or necrotic brain tumours and abscesses, but it is worth mentioning that brain tumours and abscesses can additionally be differentiated by examining their cystic components: abscess cysts exhibit Lac, lipids, acetate and various amino-acid peaks from valine, leucine, Ala and other metabolites attributable to different proteolytic enzymes, whereas "pure" tumour cysts show only resonances from Lac or lipids [22, 44], but not the variable spectral pattern of inflammatory cysts.

Infarcts showed reduction of all metabolites including Cho (Figs. 1a, 9; Table 1) and prominent Lac resonances, in general agreement with published reports [32, 45]. NAA is reduced due to loss of intact neuronal cells, and Cr is markedly diminished because of general breakdown of energy metabolism [32, 46]. Increased Cho/Cr ratios in brain infarction have been reported earlier; these authors attributed elevated Cho to a breakdown of plasma or cell membranes, which is believed to lead to an increase of free Cho in the extracellular space [45, 47]. Based on our observations, we presume that the increased Cho/Cr ratio in infarcts is secondary to a more pronounced reduction of Cr than of Cho, but not because of an elevation of Cho (Table 1; Fig. 1a). In our study, the relative signal intensities of Cho and of the other brain metabolites were clearly reduced in relation to healthy brain tissue. It is our opinion that determination of metabolite signal intensities as the proportion to the corresponding metabolite of contralateral normal brain (i.e. relative signal intensity) is superior to the calculation of metabolite/Cr ratios (e.g. NAA/Cr or Cho/Cr), since the absolute changes of metabolites are better reflected when handling the data in comparison with the "internal standard" of mirror-image healthy brain (Table 1; Fig. 1a). In addition to decreased Cho, Cr and NAA and prominent Lac resonances, there was yet another spectral hallmark typical for cerebral ischaemia: in more than 50% of infarct spectra we found an additional peak at 1.8 ppm, which is attributed to acetate, a direct degradation product of destroyed *N*-acetyl-aspartate [22, 24]. Although less frequently a diagnostic problem, cerebral infarction can be differentiated spectroscopically from low-grade astrocytoma by decreased Cho and the presence of lactate and occasionally acetate, both of which are not found in low-grade gliomas.

The diagnostic value of MRS added to MRI has not been determined until now. Our data indicate clearly

(Table 2) the additive information of MRS, which led to a significantly higher number of correct diagnoses and to a noticeably lower proportion of incorrect and equivocal diagnoses. Moreover, the additional information did not lead to incorrect diagnoses when compared with structural MRI alone. Therefore, it is concluded that the biochemical information given by ^{1}H-MRS is a useful additional diagnostic modality for preoperative grading of human gliomas, differentiating contrast-enhancing neoplastic and non-neoplastic lesions such as cerebral metastases, high-grade gliomas and abscesses, and allowing differentiation of non-contrast enhancing lesions such as low-grade gliomas from acute and subacute infarction.

Reference

1. Cecconi L, Pompili A, Caroli F (eds) (1992) MRI atlas of central nervous system tumours. Springer, Wien New York, pp 95–135
2. Dean BL, Drayer BP, Bird CR, Flom RA, Hodak JA, Coons SW, Carey RG (1990) Gliomas: classification with MR imaging. Radiology 174:411–415
3. Kazner E, Wende S, Grumme T (eds) (1989) Computed tomography and magnetic resonance tomography of intracranial tumours, 2nd edn. Springer, Heidelberg Berlin New York
4. Kondziolka D, Lunsford LD, Martinez AJ (1993) Unreliability of contemporary neurodiagnostic imaging in evaluating suspected adult supratentorial (low-grade) astrocytoma. J Neurosurg 79:533–536
5. Stack JP, Antoun NM, Jenkins JP, Metcalfe R, Isherwood I (1988) Gadolinium-DTPA as a contrast agent in magnetic resonance imaging of the brain. Neuroradiology 30:145–154
6. Miller BL (1991) A review of chemical issues in ^{1}H-NMR spectroscopy: *N*-acetyl-L-aspartate, creatine and choline. NMR Biomed 4:47–52
7. Michaelis T, Merboldt KD, Hanicke W, Gyngell ML, Bruhn H, Frahm J (1991) On the identification of cerebral metabolites in localized ^{1}H-NMR spectra of human brain in vivo. NMR Biomed 4:90–98
8. Thulborn KR, Ackerman JJH (1983) Absolute molar concentrations by NMR in inhomogeneous B1. A scheme for analysis of in vivo metabolites. J Magn Reson 55:357–371
9. Frahm J, Bruhn H, Gyngell ML, Merboldt KD, Hänicke W, Sauter R (1989) Localized high-resolution proton NMR spectroscopy using stimulated echoes: initial applications to the human brain in vivo. Magn Reson Med 9:73–93
10. Kuesel AC, Sutherland GR, Halliday W, Smith JC (1994) ^{1}H-MRS of high grade astrocytomas: mobile lipid accumulation in necrotic tissue. NMR Biomed 7:149–155
11. Ross B, Michaelis T (1994) Clinical application of magnetic resonance spectroscopy. Magn Reson Q 10:191–247
12. Ott D, Hennig J, Ernst T (1993) Human brain tumours: assessment with in vivo proton MR spectroscopy. Radiology 186:745–752
13. Poptani H, Gupta RK, Roy R, Pamdey R, Jain VK, Chhabra DK (1995) Characterization of intracranial mass lesions with in vivo proton MR spectroscopy. AJNR Am J Neuroradiol 16:1593–1603
14. Frahm J, Bruhn H, Hänicke W, Merboldt KD, Mursch K, Markakis E (1991) Localized proton NMR spectroscopy of brain tumours using short-echo time STEAM sequences. J Comput Assist Tomogr 15:915–922
15. Negendank WG, Sauter R, Brown TR, Evelhoch JL, Falini A, Gotsis ED, Heerschap A, Kamada K, Lee BC, Mengeot MM, Moser M, Padavic-Shaller KA, Sanders JA, Spraggins TA, Stillman AE, Terwey B, Vogl TJ, Wicklow K, Zimmermann RA (1996) Proton magnetic resonance spectroscopy in patients with glial tumours: a multicenter study. J Neurosurg 84:449–458
16. Herminghaus S, Möller-Hartmann W, Wittsack J, Labisch C, Dierks T, Marquardt G, Lanfermann H, Zanella FE (1998) Grading of astrocytomas using spectral pattern recognition analysis of in vivo spectroscopic data. Riv Neuroradiol 11:81–83
17. Tate AR, Griffiths JR, Martinez-Perez I, Moreno A, Barba I, Cabanas ME, Watson D, Alonso J, Bartumeus F, Isamat F, Ferrer I, Vila F, Ferrer E, Capdevila A, Arus C (1998) Towards a method for automated classification of ^{1}H-MRS spectra from brain tumours. NMR Biomed 11:177–191
18. Preul MC, Caramanos Z, Collins DL, Villemure JG, Leblanc R, Olivier A, Pokrupa R, Arnold DL (1996) Accurate, noninvasive diagnosis of human brain tumours by using proton magnetic resonance spectroscopy. Nat Med 2:323–325
19. Bottomley PA (1987) Spatial localization in NMR spectroscopy in vivo. Ann N Y Acad Sci 508:333–348
20. Tzika AA, Vigneron DB, Dunn RS, Nelson SJ, Ball WS (1996) Intracranial tumours in children: small single-voxel proton MR spectroscopy using short- and long-echo sequences. Neuroradiology 38:254–263
21. Petroff OA, Spencer DD, Alger JR, Prichard JW (1989) High field proton magnetic resonance spectroscopy of human cerebrum obtained during surgery for epilepsy. Neurology 39:1197–1202
22. Kim SH, Chang KH, Song IC, Han MH, Kim HC, Kang HS, Han MC (1997) Brain abscess and brain tumour: discrimination with in vivo H-1 MR spectroscopy. Radiology 204:239–245
23. Tien RD, Lai PH, Smith JS, Lazeyras F (1996) Single-voxel proton brain spectroscopy exam (Probe/SV) in patients with primary brain tumours. AJR Am J Roentgenol 167:201–209
24. Duijn JH, Matson GB, Maudsley AA, Hugg JW, Weiner MW (1992). Human brain infarction: proton MR spectroscopy. Radiology 183:711–718
25. Barker PB, Glickson JD, Bryan N (1993) In vivo magnetic resonance spectroscopy of human brain tumours. Top Magn Reson Imaging 5:32–45
26. Felber SR (1993) ^{1}H magnetic resonance spectroscopy in intracranial tumours and cerebral ischemia. Radiologe 33:626–632
27. Gill SS, Thomas DG, Van Bruggen N, Gadian DG, Peden CJ, Bell JD, Cox IJ, Menon DK, Iles RA, Brynant DJ (1990) Proton MR spectroscopy of intracranial tumours: in vivo and in vitro studies. J Comput Assist Tomogr 14:497–504
28. Sutton LN, Wang Z, Gusnard D, Lange B, Perilongo G, Bogdan AR, Detre JA, Rorke L, Zimmermann RA (1992) Proton magnetic resonance spectroscopy of pediatric brain tumours. Neurosurgery 31:195–202
29. Kugel H, Heindel W, Ernestus RI, Bunke J, du Mesnil R, Friedmann G (1992) Human brain tumours: spectral patterns detected with localized H-1 MR spectroscopy. Radiology 183:701–709

30. Go KG, Kamman RL, Mooyaart EL, Heesters MA, Pruim J, Vaalburg W, Paans AM (1995) Localised proton spectroscopy and spectroscopic imaging in cerebral gliomas, with comparison to positron emission tomography. Neuroradiology 37:198–206
31. Alger JR, Frank JA, Bizzi A, Fulham MJ, DeSouza BX, Duhaney MO, Inscoe SW, Black JL, van Zijl PC, Moonen CT (1990) Metabolism of human gliomas: assessment with H-1 MR spectroscopy and F-18 fluorodeoxyglucose PET. Radiology 177:633–641
32. Lanfermann HL, Kugel H, Heindel W, Herhorz K, Heiss WD, Lacker K (1995) Metabolic changes in acute and subacute cerebral infarctions: Findings at proton MR spectroscopic imaging. Radiology 196:203–210
33. Tedeschi G, Lundbom N, Raman R, Bonavita S, Duyn JH, Alger JR, Di-Chiro G (1997) Increased choline signal coinciding with malignant degeneration of cerebral gliomas: a serial proton magnetic resonance spectroscopy imaging study. J Neurosurg 87:516–524
34. Demaerel P, Johannik K, Van Hecke P, Van Ongeval C, Verellen S, Marchal G, Wilms G, Plets C, Goffin J, Van Calenbergh F (1991) Localized ^{1}H-NMR spectroscopy in fifty cases of newly diagnosed intracranial tumours. J Comput Assist Tomogr 15:67–76
35. Sijens PE, Levendag PC, Vecht CJ, van Dijk P, Oudkerk M (1996) ^{1}H MR spectroscopy detection of lipids and lactate in metastatic brain tumours. NMR Biomed 9:65–71
36. Meyerand ME, Pipas JM, Mamourian A, Tosteson TD, Dunn JF (1999) Classification of biopsy-confirmed brain tumours using single-voxel MR spectroscopy. AJNR Am J Neuroradiol 20:117–123
37. De Stefano N, Caramanos Z, Preul MC, Francis G, Antel JP, Arnold DL (1998) In vivo differentiation of astrocytic brain tumours and isolated demyelinating lesions of the type seen in multiple sclerosis using ^{1}H magnetic resonance spectroscopic imaging. Ann Neurol 44:273–278
38. Sallinen PK, Sallinen SL, Helen PT, Rantala IS, Rautisinen E, Helin HJ, Kalimo H, Haapasalo HK (2000) Grading diffusely infiltrating astrocytomas by quantitative histopathology, cell proliferation and image cytometric DNA analysis. Comparison of 133 tumours in the context of the WHO 1979 and WHO 1993 grading schemes. Neuropathol Appl Neurobiol 26:319–331
39. Tamiya T, Kinoshita K, Ono Y, Matsumoto K, Furuta T, Ohmoto T (2000) Proton magnetic resonance spectroscopy reflects cellular proliferative activity in astrocytomas. Neuroradiology 42:333–338
40. Mountford CE, Mackinnon WG, Bloom M, Burnell EE, Smith IC (1984) NMR methods for characterizing the state of surfaces of complex mammalian cells. J Biochem Biophys Methods 9:323–330
41. Mountford CE, Saunders JK, May GL, Holmes KT, Williams PG, Fox RM, Tattersall MH, Barr JR, Russell P, Smith IC (1986) Classification of human brain tumours by high-resolution magnetic resonance spectroscopy. Lancet 1:651–653
42. Malycha P, Mountford C (1998) Magnetic resonance spectroscopy and breast cancer. Aust N Z J Surg 68:859–862
43. Gupta RK, Poptani H, Kohli A, Chhabra DK, Sharma B, Gujral RB (1995) In vivo localized proton magnetic resonance spectroscopy of intracranial tuberculomas. Indian J Med Res 101:19–24
44. Schumacher DJ, Nelson TR, van Sonnenberg E, Meng TC, Hlavin P (1992) Quantification of amino acids in human body fluids by ^{1}H magnetic resonance spectroscopy: a specific test for the identification of abscess. Invest Radiol 27:999–1004
45. Kamada K, Houkin K, Iwasaki Y, Abe H, Kashiwaba T (1997) Metabolic and neurological patterns in chronic cerebral infarction: a single voxel ^{1}H-MR spectroscopy study. Neuroradiology 39:560–565
46. Bruhn H, Frahm J, Gyngell ML, Merboldt KD, Hanicke W, Sauter R (1989) Cerebral metabolism in man after acute stroke: new observation using localized proton NMR spectroscopy. Magn Reson Med 9:126–131
47. van den Grond J, Balm R, Kapelle LJ, Eikelboom BC, Mali WP (1995) Cerebral metabolism of patients with stenosis or occlusion of the internal carotid artery. A ^{1}H-MR spectroscopic imaging study. Stroke 26:822–828